A structural study of the complex between neuroepithelial cell transforming gene 1 (Net1) and RhoA reveals a potential anticancer drug hot spot

Petit, Alain-Pierre; Garcia-Petit, Christel; Bueren-Calabuig, Juan A; Vuillard, Laurent M; Ferry, Gilles; Boutin, Jean A

Published in:
Journal of Biological Chemistry

DOI:
10.1074/jbc.RA117.001123

Publication date:
2018

Document Version
Peer reviewed version

JBC Papers in Press. Published on April 25, 2018 as Manuscript RA117.001123
The latest version is at http://www.jbc.org/cgi/doi/10.1074/jbc.RA117.001123

A structural study of the complex between neuroepithelial transforming gene 1 (Net1) and RhoA reveals a potential anti-cancer drug hotspot

Alain-Pierre Petit[1], Christel Garcia-Petit[2], Juan A. Bueren-Calabuig[1], Laurent M. Vuillard[3], Gilles Ferry[3], Jean A. Boutin[3*]

[1]Drug Discovery Unit, Division of Biological Chemistry and Drug Discovery, School of Life Sciences, University of Dundee, Dundee, UK
[2]MRC Protein Phosphorylation and Ubiquitylation Unit, School of Life Sciences, University of Dundee, Dundee DD1 5EH, UK
[3]Pôle d'Expertise Biotechnologie, Chimie, Biologie, Institut de Recherches SERVIER, 78290 Croissy-sur-Seine, France

*To whom correspondence should be addressed at Dr. Jean A. Boutin: jean.boutin@servier.com

Running title: Druggable rhoA/Net1 interface

Keywords: Small GTPases; PPI; rhoA; Net1; peptides; crystallization; heterodimer structure

ABSTRACT

The GTPase RhoA is a major player in many different regulatory pathways. RhoA catalyzes GTP hydrolysis, and its catalysis is accelerated when RhoA forms heterodimers with proteins of the guanine nucleotide exchange factor (GEF) family. Neuroepithelial cell transforming 1 (Net1) is a RhoA-interacting GEF implicated in cancer, but the structural features supporting the RhoA/Net1 interaction are unknown. Taking advantage of a simple production and purification process, here we solved the structure of a RhoA/Net1 heterodimer with X-ray crystallography at 2 Å resolution. Using a panel of several techniques, including molecular dynamics simulations, we characterized the RhoA/Net1 interface. Moreover, deploying an extremely simple peptide-based scanning approach, we found that short peptides (penta- to nona-peptides) derived from the protein–protein interaction region of RhoA could disrupt the RhoA/Net1 interaction and thereby diminish the rate of nucleotide exchange. The most inhibitory peptide, EVKHF, spanning residues 102–106 in the RhoA sequence, displayed an IC50 of ~100 µM, without further modifications. The peptides identified here could be useful in further investigations of the RhoA/Net1 interaction region. We propose that our structural and functional insights might inform chemical approaches for transforming the pentapeptide into an optimized pseudopeptide that antagonizes Net1-mediated RhoA activation with therapeutic anticancer potential. Rho GTPases control many aspects of cell behavior, such as cytoskeleton organization, cell-cycle progression, and gene transcription (1, 2). The dysregulation of Rho proteins contributes to tumorigenesis, metastasis (3), hypertension (4, 5), diabetes (6, 7), inflammation (8), neuroplasticity (9), and cancer (3). Thus, targeting Rho GTPase signaling pathways has emerged as a promising therapeutic strategy (10, 11).

In human, 22 genes encode Rho GTPase family members. Three members, RhoA, Cdc42, and Rac1, are the best characterized, and they illustrate the key functions of the family (12–15). GTPases are molecular switches that cycle between the active GTP-bound state and, after GTP hydrolysis, the inactive GDP-bound state.

In the active state, they recognize target proteins and induce cellular responses. Two classes of proteins are mainly involved in Rho regulation. One class comprises GTPase-activating proteins (GAPs), which suppress Rho signaling by enhancing Rho GTPase activity. The other class comprises guanine nucleotide-exchange factors (GEFs), which promote Rho activity by catalyzing the exchange of GDP for GTP (16).

Neuroepithelial transforming gene 1 (Net1) is a GEF specific for RhoA (17) and RhoB (18). Net1 is a protein of 596 amino acids, with two tandem domains, one with Dbl Homology (DH) and the other with Pleckstrin Homology (PH), which are flanked by amino-terminal and carboxyl-terminal extensions. The DH-PH domain, present in most GEFs, provides the minimal structural unit required to catalyze the nucleotide exchange reaction *in vivo*. Net1 shuttles between the nucleus and the plasma membrane in response to cell-motility stimuli. Furthermore, Net1 is overexpressed in a number of human cancers, particularly gastric adenocarcinoma (19, 20). Through RhoA activation, Net1 stimulates cell motility, invasion, and cell spreading in response to a variety of ligands. The cytoskeletal rearrangements driven by Net1 comprise a key pathological mechanism in gastric tumor cell migration and extracellular matrix invasion (21, 19). Elevated Net1 expression levels were shown to correlate with the progression of tumors, such as hepatocellular carcinoma (22) and lung cancers (23).

The unique role of Net1 in tumor cell migration through its interaction with RhoA has focused interest on the RhoA/Net1 interface as a potential target for anti-cancer drugs. Previously, drug discovery campaigns attempted to target the structurally conserved interface between GEFs and RhoA. However, due to the limited binding specificity of Rhos and GEFs, those approaches have led to molecules with severe selectivity issues (24). From the purely molecular point of view, a few key papers have described the relationship between RhoA and GEF 11 or GEF 12 (25–28), but little is known regarding the interface between RhoA and Net1.

Therefore, we aimed to gain more structural information, both on the RhoA/Net1 interface and on the complex. In the present work, we solved the crystal structure of the Net1/RhoA complex with X-ray crystallography. Then, with molecular modeling and enzymatic assays, we identified the residues that contributed most of the energy required to form the Net1-PH/RhoA interaction. Based on these calculations, we determined the molecular recognition process. Finally, we designed small peptides that could inhibit the guanine exchange activity by disrupting the Net1-PH/RhoA interface.

RESULTS & DISCUSSION

Purification of the Net1/RhoA complex. Initially, we purified the $Net1^{DHPH}$ domain, which comprised residues 157-494 and a hexahistidine (His_6) plus a TEV tag at the N-terminus. This protein was expressed well, and it could be purified in two chromatography steps (Ni NTA affinity and gel filtration). However, it did not show any nucleotide exchange enhancing activity. Hence, we extended the C-terminus to residue 501 (157-501) and added a C-terminal His_6 tag, which restored some GEF activity. Then, we altered the N-terminus to start at either residue 149 or 170. These final constructs exhibited higher GEF activity. We used 149-501 with a His_6 C-terminal tag for crystallography. RhoA was prepared as described previously (25). These recombinant proteins were mixed, dialysed, and further purified to yield a fair amount of protein amenable to crystallography grade material (**Figure 1**). The quality of the preparation was a key factor in the next steps of this study. Indeed, although not unique (25, 26, 29), purifications of this type are not common.

Overall structure of the $Net1^{DHPH}$/RhoA complex. The asymmetric unit had two heterodimers of $Net1^{DHPH}$/RhoA. The heterodimers were identical as indicated by the low RMSD value (0.4 Å or 0.45 Å, with RhoA or Net1 as references, respectively). Net1 contained the DH and PH domains. The DH domain was an oblong helical bundle; it facilitates nucleotide exchange by forming a stable

complex with the nucleotide-free conformation of the RhoA GTPase. The PH domain was a flattened, 7-standed, B-barrel, capped with a characteristic C-terminal α-helix (αC). The broad picture is like what has been described for other RhoGEF complexes with a RhoA (30), devoid of nucleotide and with a large interface (**Figure 2**)

In our structure, RhoA was clamped between the DH and PH domains of Net1. This conformation was cation- and nucleotide-free, with switch I removed from the nucleotide-binding site and switch II pulled towards the nucleotide-binding site. This conformation was similar to those previously reported for RhoA/GEF complexes, where the interaction with the DH/PH domains stabilized the nucleotide-free form of RhoA by altering the structures of the two switches.

A superposition of this RhoA with the structure of RhoA in complex with a nucleotide indicated a likely binding site for the nucleotide in the RhoA/Net1 complex. Indeed, we reasoned that the nucleotide was likely to bind to the active site through an extensive network of hydrogen bonds, including residues G17, K18, and T19, which could interact with the pyrophosphate group. Additionally, residues K118, D120**,** A161, and K162 could interact with the guanosine moiety (**Figure 3**). The cation-π interaction between the guanine and K118 is conserved among RhoA structures solved in presence of nucleotide. In our structure, the conformation of the RhoA active site was nearly identical to that described previously, for RhoGEF12 (RhoGEF12; RMSD 1.1 Å with RhoA: PDB code **1X86**) (26). In particular, the orientation of the loop near the G14 residue, critical for GTP binding, was similar in these two structures; the lateral chain pointed towards the nucleotide-binding site, and thus, preventing nucleotide binding. The 160-165 loop was significantly reorganized, which allowed the formation of hydrogen bonds between the guanine and A161 and K162. This conformation was observed previously in the structure of Rho/GEF11 (PDB code **1XCG)** (25).

*Comparison of the Net1^{DHPH} (**4XH9**) and Net1^{DH} (**3EO2**) structures.* The crystal structure of the DH domain was previously solved with a resolution of 2.6 Å (PDB code **3EO2**). The RMSD analysis calculated for the main chains of Net1^{DHPH} (PDB code **4XH9**) and Net1^{DH} (PDB code **3EO2**) pointed out that residues 280-310 were severely deviated in Net1^{DH} (**Figure 4A**). Upon RhoA binding, the N-terminal domain of NET1^{DHPH} was shifted by ~40 degrees compared to Net1^{DH} (**Figure 4B**); this shift prevented steric clashes between residues S306 and D309 on Net1 and W58 on RhoA (**Figure 4C**). A consequence of this reorganization was the displacement of the 284-295 alpha helix, induced by the H-bond formed between W305 of Net1^{DHPH} and L72 of RhoA.

The DH/RhoA interface. All the interactions between Net1^{DHPH} and RhoA were conserved in the two complexes of the asymmetric unit. Twelve amino acids in RhoA, distributed between R5 and S73, were involved in polar interactions with DH. Moreover, E40, D45, and E76 in RhoA established salt bridges with K317, K301 and K274 in DH (**Figures 5A & B**). Residues V38, V43, W58, and Y66 in RhoA and L321, L302, W305, and L350 in DH were involved in hydrophobic interactions (within 4 Å). With the PISA server, we found the closest homologues available in the RCSB data bank, based on interface homology. The most significant homologues for which a similar interface was previously described were RhoA/GEF12 (PDB code **1X86**) (26) and RhoA/GEF11 (PDB code **1XCG**) (25). Despite a rather low sequence homology between these two RhoGEF proteins, many of the residues involved in the interactions with RhoA were conserved. There are nevertheless original contacts in the case of Net1 as shown in **Table 1**.

The PH/RhoA interface. X-ray crystallography models were supplemented with molecular dynamics simulations to provide insight into the dynamic properties and conformational changes of the RhoA/Net1 complex. We found that the presence of RhoA strongly influenced the conformational dynamics of the Net1 PH domain (**Figures 6A, B**). In complex with RhoA, the N-terminal

domain of the α6-helix of Net1 PH remained stable, in a position similar to that observed in the crystal structure (RMSD=1Å), and the PH/DH domain angle remained constant at approximately 125º **(Figure 6A**). On the other hand, in the RhoA-free system, Net1 samples displayed multiple conformal states (**Figure 6B**). The absence of the Net1-RhoA interaction increased the flexibility of α6-helix, which altered the position of the PH domain.

No RhoA guanine nucleotide exchange could be detected with the isolated DH domain in the *in vitro* exchange assay (**Figure 7**). Thus, we concluded that the presence of the PH domain was critical to the activity of Net1, and that it must be stabilized in the interaction with RhoA.

In the Rho/GEF11 and Rho/GEF12 crystal structures, the binding of PH to RhoA is mediated by two forces. One is a hydrogen bond between E97 in RhoA and S1118/S1065 in PH; the other is a salt bridge formed by R68 in RhoA with either E1023 or E969 in PH (**Figure 8A**). This binding mode was not observed in the $Net1^{DHPH}$/RhoA structure, which suggested that the Net1 PH domain must be stabilized in a unique way. We found that, in the $Net1^{DHPH}$/RhoA crystal structure, the H105 residue in RhoA bridged the water molecule, WATER1, which was further stabilized by E392, W492, and H488 in the Net1 PH domain. RhoA H105 also interacted with the H390 amide group, either directly or with the mediation of water (WATER2). The imidazole ring formed both a salt bridge with E361 in the DH domain (known as the DHPH intrachain interaction) and a π-π interaction with the Y365 phenyl ring (**Figure 8B**). The existence of this unique mode of interaction was supported by low values of the b factors, calculated after isotropic refinement, and the RMSD of the residues/waters measured in the molecular dynamics simulations (**Table 2**).

$Net1^{PH}$ was later purified to investigate the *in vitro* formation of the $Net1^{PH}$/RhoA heterodimer. First, the folding of $Net1^{PH}$ was confirmed with 1H NMR. The NH signals in the range of ~8.00 to 9.6 PPM and signals down to -0.5 PPM matched the aromatic and the aliphatic regions of the spectrum (**Figure 9A**). This result indicated the presence of folding in the structure. The abundance of signals in the region of 8.5 PPM may indicate the presence of unfolded regions in the PH domain. The interaction between $Net1^{PH}$ and RhoA was analyzed by gel filtration chromatography (**Figure 9B**) and SDS-PAGE electrophoresis (**Figure 9C**). Despite different ratios of $Net1^{PH}$ to RhoA (1:1 and 2:1), we observed no dimer formation, as indicated by the lack of $Net1^{PH}$ in the eluted fractions of high molecular weights. Consequently, we concluded that the binding of $Net1^{PH}$ to RhoA was most likely induced by the binding of Net1-DH to RhoA. Alternatively, one might consider that the interaction of Net1PH (i.e. without its DH domain) with RhoA is too weak to have been detected by the methods used.

Targeting the PH/RhoA interface with small peptides. The previous finding that Net1 played a role in metastatic processes served as an incentive to target it. Early attempts to target a specific GEF DH/RhoA interface led to non-specific inhibition, due to the fact that the DH/RhoA interface is highly conserved among GEFs. Therefore, we reasoned that the unique Net1-PH/RhoA interface may provide a selective target for altering the cellular effects of Net1. However, targeting protein–protein interactions has long been considered highly challenging, due to their large, dynamic interfaces. To address these challenges, we employed computational approaches to design small peptides that mimicked the key Net1-RhoA interface interactions.

We used a decomposition approach that combined molecular mechanics energies with the generalized Born and surface area continuum solvation (MM-GBSA) to identify the residues that made the most important energetic contributions to the formation of the PH domain/RhoA complex (**Figure 10A, B**). Residues D485 to Q491 in Net1 contributed significantly to the binding free energy of the complex. This segment established multiple interactions with residues 100 to 106 in RhoA. In particular, D485 and H488 (Net1) formed several hydrogen bonds and salt bridges with K104 and H105 (RhoA).

As a result of this analysis, we identified potential hotspots involved in the binding between Net1 and RhoA. This information allowed us to initiate competition assays with peptides derived from the loops of contact in RhoA. Peptides that mimicked potential hot-spots in segment 96 to 106 of RhoA were designed to perturb the $Net1^{DHPH}$/RhoA interface. We monitored the inhibition of guanine nucleotide exchange to identify hot-spots that affected function (**Figure 11A, B**). Competitive assays performed with peptide 96-102 that formed the RhoA "hydrophobic pocket" showed no inhibition efficiency in the molecular dynamics analysis. In contrast, a short peptide that spanned amino acids 102 to 106 exhibited an IC50 of 116.5 ± 6.3 µM (**Figure 11 C**). Longer peptides (96-106 or 100-109) display poor inhibition effect, suggesting folding/aggregation issues. Finally, no inhibition of Net1 was measured when peptide 100-105, devoid of the phenyalanine F106, was used.

This finding indicated that the stabilization of PH on RhoA was mediated by a limited number of residues in the 102-106 segment of RhoA. Next, we estimated the selectivity of peptide 102-106 inhibition by measuring its effect on the guanine exchange activity of the two closest homologues of Net1: GEF3 and GEF12 (16) (**Figure 12A & B**). We found that 0.5 mM of peptide 102-106 did not significantly inhibit GEF3 and GEF12 activities. The inefficient effect of peptide 102-106 on GEF12 could be explained by the difference in the PH/RhoA interfaces observed in the crystal structures. The inability of peptide 102-106 to inhibit GEF3 was unexpected, because the Net1 and GEF3 sequences varied by only a single amino acid in this region where both proteins seem to interact (His488 in Net1 vs. Asn436 in GEF3; **Figure 13**). This finding suggests that His488 is a driving residue for the peptide recognition and the selectivity process. To confirm this hypothesis, the activities of mutated Net1 (H488A and H488N) and GEF3 (N436H) were measured in the presence of the peptide 102-106. Mutation of H488N or of H488A made NET1 insensitive to the peptide 102-106 whereas sensitivity to the peptide was partially restored for the mutated GEF3 N436H (**Figure 14**). These results confirmed that i) the peptide mimics the binding of RhoA to Net1 PH domain and that ii), the selectivity is driven by the residue H488.

To summarize, a hot-spot has been identified at the Net1/RhoA interface and structure-activity analysis of key residues of the peptide 102-106 (EVKHF) led to the identification of three functional groups that will help to generate pharmacophore models representing all necessary functional properties in the appropriate spacing and 3-D orientation required to facilitate compound optimization: a scaffold (made by the H105 imidazole ring), a hydrophobic pocket suitable to improve the lipophilic properties during the lead generation (F106 phenyl ring) as well as an array to develop the compound selectivity (toward the targeting of Net1 H488).

As a conclusion, the search for new approaches for identifying molecules for fighting cancer remains dramatically important. Gaining a better understanding of the molecular nature of relationships that regulate protein-protein interactions will facilitate achieving this goal. However, when the target of interest is neither an enzyme nor a receptor, the nature of the protein-protein interaction that regulates the complex is often a flat surface, where hotspots are either difficult to find or simply do not exist (31). An abundance of technologies have been described in the last few years, which have facilitated the achievement of this difficult task. In some cases, those efforts have provided patients with less toxic, more specific, tolerable compounds, and ultimately drugs (32). Consequently, it is recommended that three paradigms should be revisited: (i) finding specific proteins involved in subclasses of diseases; (ii) improving the descriptions, and thus, the understanding of protein-protein interactions at the molecular level (33, 34); and (iii) demonstrating that even 'flat' surfaces can be druggable, particularly with peptides or macrocycles, which are good starting points for that type of discovery program (35). Here, we used a

simple biochemical approach to produce the two partners of the Net1/RhoA complex. This study was the first to solve their co-crystal structure, and thus, the structure of this type of complex. From there, we used modern molecular dynamics tools to describe the behavior of the complex and the nature of the interface between these proteins. Then, we designed short peptide sequences and showed that small sequences could interfere with the interaction between RhoA and Net1, which led to the impairment of RhoA catalytic activity. Although much remains to be undertaken before reaching patients, these results exemplified the technical and strategic avenues that can lead to progress.

EXPERIMENTAL PROCEDURES.

Reagents and peptides. All reagents used in the present work were of analytical grade or better. Peptides were custom-synthesized by Genepep (St Jean de Vedas, France). In brief, they were synthesized with the solid-phase synthesis method, cleaved off the resin, purified, and thoroughly analyzed with HPLC and mass spectrometry. Peptide purity was systematically higher than 98%, judged by both techniques.

Plasmids and recombinant proteins. Two plasmids were constructed, one carried the sequence encoding human RhoA (residues 2-180), with a F25N mutation, and the other carried the sequence encoding human Net1 (residues 149-501). Both constructs were cloned into pET28 and expressed in *Escherichia coli* BL21 RIL (DE3) cells as His_6-tagged proteins (an N-terminal tag, plus a TEV cleavage site for RhoA, and a C-terminal tag for Net1). The cells were grown overnight at 17°C in auto-inducing media (36). Cells were harvested by centrifugation and resuspended in lysis buffer (50 mM Tris pH8, 250 mM NaCl, 10% (w/v) glycerol, 10 mM MgCl2, 1 mM PMSF, 20 mM MgSO4) in the presence of 10 mg DNAse and 250 mg/L lysozyme per liter of buffer. During the isolation of RhoA, all buffers, from lysis to the final purification step, were supplemented with 50 µM GDP. The proteins were purified independently, but in a similar fashion, on His Trap FF crude columns (5 mL). After loading the sample, the column was washed with 20 volumes of wash buffer (50 Tris mM pH8, 250 mM NaCl, 10 mM MgCl2, 50 µM GDP, 10% (w/v) glycerol). The protein was eluted with 50 mM Tris pH8, 250 mM NaCl, 10 mM MgCl2, 10% (w/v) glycerol, and 250 mM imidazole.

For RhoA purification, the protein was then desalted in 20 mM Tris pH8, 250 mM NaCl, 2 mM DTT, 5% glycerol, 1 mM MgCl2, 50 µM GDP, and cleaved overnight with TEV protease at 4°C. The sample was then passed through a His trap FF column equilibrated with cleavage buffer. Next, the sample was concentrated to 5 mg/mL. The protein was purified with gel filtration chromatography (Superdex 200 26/60, GE Healthcare) in 20 mM Tris pH8, 10 mM HCl, 250 mM NaCl, 2 mM DTT, 5% glycerol, 1 mM MgCl2, and 50 µM GDP.

For Net1 isolation, after histrap FF purification step, $Net1^{DHPH}$ was directly purified with gel filtration chromatography (Superdex 200 26/60, GE Healthcare) in 20 mM Hepes pH7.5, 150 mM NaCl, 5% (w/v) glycerol, 2 mM DTT.

The Net-Rho complex was produced by incubating GDP-loaded RhoA with $Net1^{DHPH}$ at a molar ratio of 2:1 for 10 min, followed by overnight dialysis in 20 mM Tris pH7.1, 150 mM NaCl, 5 mM EDTA, 1 mM TCEP. A final gel filtration step (Superdex 75 26/60, GE Healthcare), in 20 mM Tris pH7.2, 150 mM NaCl, 1 mM TCEP (**Figure 1**), was used to isolate the RhoA-$Net1^{DHPH}$ complex from free RhoA. The complex was concentrated to 12 mg/mL, and this sample was used for crystallization experiments.

Protein purification. Net1 (residues 149-501) H488N, Net1 (residues 149-501) H488A and DH domain (residues 149 to 370). The Net1 sequence encoding residues 149-370 was cloned into the pET15 plasmid and expressed in *E. coli* BL21 (DE3) cells as a His_6-tagged protein (N-terminal tag with a TEV cleavage site). H488A or H488N mutation was inserted following the QuikChange II Site-Directed Mutagenesis (Agilent technologies) procedure.

Cells were grown in auto-inducing media at 20°C. Net1_DH, Net1 H488N and Net1

H488A were purified with the procedure described above for Net1-149-501.

Protein purification. PH domain (residues 358 to 501). The Net1 sequence encoding residues 358-501 was cloned into the pET15 plasmid and expressed in *E. coli* BL21 (DE3) cells as a His_6-Maltose Binding Protein (MBP) tagged protein (N-terminal tag with a TEV cleavage site). Cells were grown in LB media at 17°C after induction with 0.1 mM isopropyl β-D-1-thiogalactopyranoside (IPTG). Harvested cells were re-suspended in a lysis buffer of 50 mM Tris, 200 mM NaCl, 10% glycerol, 1 mM TCEP, pH7.5, supplemented with DNAse and anti-proteases. Cells were lysed at 30 psi with a cell disruptor. Net1_358-501 was initially purified with affinity chromatography in 50 mM Tris, 200 mM NaCl, 10% glycerol, 1 mM TCEP, pH7.5 ±500 mM imidazole. Then, it was purified with the procedure described above for Net1_149-501. Fractions of interest were further purified with gel filtration chromatography on a Superdex 75 26/60, pre-equilibrated with 50 mM Tris, 200 mM NaCl, 10% glycerol, 1 mM TCEP pH7.5. Pure fractions were pooled and incubated with 1/20 TEV overnight at 4°C under slow agitation. The mixture was diluted (×4) in Hepes 50 mM, 10% glycerol, 1 mM TCEP pH 7.3, to achieve a final concentration of 50 mM NaCl. The sample was then loaded on a Hi Trap SP column (5 mL) that had been pre-equilibrated in 50 mM Hepes, 50 mM NaCl, 10% glycerol, 1 mM TCEP pH 7.3 at a flow rate of 6 mL/min. Flow-through fractions were saved. Elution was performed with a salt gradient (50 to 500 mM) in 35 min at a flow rate of 2 mL/min.

Protein purification. ARHGEF3 (residues S94 to E449) and ARHGEF3 (residues S94 to E449) N436H. The gene encoding the DH-PH domain (S94-E449) of *H. sapien GEF3* was cloned into the pET15 vector as a His_6-tagged protein (C-terminal tag) and expressed in *E. coli* BL21 (DE3) cells in auto-induction media at 17°C. N436H mutation was inserted following the QuikChange II Site-Directed Mutagenesis (Agilent technologies) procedure. ARHGEF3 (WT and N436H) were purified with the procedure described above for Net1-149-501.

Protein purification. ARHGEF12 (residues N768 to S1138, with a Y973F mutation). The gene encoding the DH-PH domain (N768-S1138) of *H. sapien GEF12* was cloned into the pET15 vector with both an MBP-tag (N-terminal tag with TEV) and a His_6-tag (C-terminal tag). The protein was expressed in *E. coli* BL21 RIL (DE3) cells in auto-induction media at 17°C. ARHGEF12 was initially purified with affinity chromatography, according to the procedure described above for Net1_149-501. Then, samples containing ARHGEF12 were pooled and immediately dialysed overnight at 4°C in the presence of TEV protease (1/20) against 50 mM Tris, 200 mM NaCl, 10% glycerol, 1 mM TCEP pH7.5. Samples were then passed through a HisTrap HP (5 mL) Ni-NTA column and eluted with a gradient of 5 to 50% B (Buffer supplemented with 500 mM imidazole) in 50 min at a flow rate of 2 mL/min. Fractions of interest were applied to a Superdex 75 26/60 column (GE Healthcare) that had been pre-equilibrated with 50 mM Tris, 200 mM NaCl, 10% glycerol, 1 mM TCEP, pH 7.5.

^{1}H-NMR analysis of Net1^{PH} domain (residues 358 to 501). A 200 µL volume of protein was brought to a concentration of 1.8 mg/mL (104.8 µM) in 20 mM Tris, 200 mM NaCl, 10% glycerol, 1 mM TCEP pH 7.5. This solution was mixed with 20 µL D2O (Cambridge Isotopes Laboratory) and placed in a 3 mm NMR tube (Wilmad 307-PP-7). The NMR experiment was performed at 20°C on a Bruker AVANCE III HD spectrometer equipped with a QCI-F cryoprobe, operating at 500.13 MHz. The spectrum was analyzed with the TopSpin 3.2 program. Protein folding was evaluated, based on the presence of a wide range of NH signals in the region of 8.0 to 9.6 ppm and aliphatic signals in the region of -0.6 to 0.5 ppm.

Analysis of the dispersion of the NMR signals in the regions of the methyl protons (0.5 to 1.5 ppm), -alpha-protons (3.5– 6 ppm), and amide protons (6–10 ppm) confirmed the folding of the Net1^{PH} purified protein (37).

Analytic gel filtration chromatography of the Net^{PH} domain/RhoA complex. Retention profiles of Net1^{PH} in presence or absence of RhoA were analyzed with gel

filtration chromatography. As controls, 7 nmoles of Net1^{PH} and 7 nmoles of RhoA were loaded on a Superdex 75 10/300 GL that had been pre-equilibrated in 20 mM Tris, 100 mM NaCl, 5% glycerol, 0.5 mM TCEP pH7.5. To analyze the complex, 7 nmoles of Net1^{PH} and 7 nmoles of RhoA were preincubated for 2 h at 4°C before the gel filtration analysis. A ratio of 2:1 was also analyzed with the same procedure, by mixing 20 nmoles of Net1^{PH} with 10 nmoles of RhoA.

Crystallization and structure determination. The RhoA-Net1^{DHPH} complex was crystallized at 20°C with the hanging drop vapor diffusion method. Crystals appeared overnight in drops composed of 1 µL protein solution mixed with 1 µL of the reservoir solution, which contained 0.1 M Bis-tris propane pH 7.5, 20% PEG3350, and 0.2 M tripotassium phosphate. Crystals were flash-frozen in the reservoir solution supplemented with 15% glycerol. Data were collected at 100 K (after annealing) from the synchrotron radiation beamline, ID23 (ESRF, Grenoble, France). Data were processed with the XDS program (38) and scaled with the SCALA program in the CCP4 suite (39). The initial phase information was obtained by performing molecular replacement with Phaser, from the CCP4 suite, and a model built from our own crystal structure of the apo Net1^{DH} domain (data not shown) combined with RhoA. The initial densities were improved further by applying solvent flattening and histogram matching with RESOLVE from the Phenix suite (40, 41). Then, the PH domain of Rho GEF 3 (PDB code **2Z0Q**) was density-fitted with Phaser to improve the density map of the DH domain. The model was finally improved by applying iterative cycles of model building and refinement with COOT (42) and Refine (Phenix suite) (40, 41). Here, we present the data measurements (**Table 3**) and model refinement statistics (**Table 4**). Coordinate files and associated experimental data have been deposited in the Protein Data Bank (PDB); accession code 4XH9.

Molecular modeling and simulations. Molecular modeling and simulation protocols were used to study, in atomic detail, the structural stability of Net1. The following systems were simulated: *i*) Net1 and *ii*) the Net1/RhoA complex. Each system was built with a template of our crystal structure of Net1 in complex with RhoA. Missing loops were modeled with the SWISS-MODEL web interface (43). Hydrogen atoms were added to the protein with the web-based H++ server, which assigned protonation states to all titratable residues at the chosen pH of 7.0 (44). Each system was immersed in a TIP3P water box (45) and neutralized with the appropriate number of counter ions (46).

Molecular dynamics simulation protocols. Standard molecular dynamics simulations were performed with the pmemd.cuda module provided in the AMBER14 suite of programs (47), with the ff14SB force field (48). The cut-off distance for the non-bonded interactions was 10Å, and periodic boundary conditions were applied. Long-range electrostatic interactions were treated with the particle mesh Ewald method (49). The SHAKE algorithm was applied to all bonds involving hydrogens (50), and an integration step of 2-fs was used throughout. Each system was studied with two 100-ns replicas of unrestrained molecular dynamics simulations, run at a constant temperature (300 K) and pressure (1 atm) with the weak-coupling algorithm (51).

Analysis methods. Three-dimensional structures were inspected with the computer graphics programs, PyMOL (52) and VMD (53). Interatomic distances, angles, and RMSDs were monitored with the "cpptraj" module in AmberTools15 (47). The last 80 ns of the molecular dynamics trajectories of each system were used to construct two-dimensional normalized density maps. The maps showed the conformational states of Net1 in the presence and absence of RhoA, based on two selected collective variables. The first variable, *'x'*, corresponded to the RMSD of the backbone atoms of residues 357-368. It was calculated after aligning only residues 158-354 of the DH domain; the crystal structure of Net1 in complex with RhoA (PDB entry **4XH9**) was used as reference. The second variable, *'y'*, corresponded to the DH-PH angle; i.e., the

angle between the alpha carbons of residues Q337, L355 (DH domain), and I496 (PH domain). We identified the dominant residues that contributed energy to the formation of the Net1-PH/RhoA complex by calculating the binding free energies of the complex with the MM-GBSA per-residue decomposition analysis, as implemented in the MMPBSA.py software (54).

Guanine nucleotide exchange assay. *In vitro* nucleotide exchange assays measured the increase in fluorescence emitted over time, upon incorporation of free Mant-GTP into a GDP-loaded RhoA molecule. To analyze the inhibition of the GDP/mant-GTP exchange reaction, the time course of the change in fluorescence was recorded in the presence of increasing concentrations of peptides (0.03 to 0.5 mM). The peptide and 1 µM RhoA were mixed at 25°C in 100 µL of 20 mM Hepes pH 7, 150 mM NaCl, 1 mM MgCl2, 1 µM mant-GTP. The reaction was initiated with the addition of 1 µM Net1 or 10 µM ARHGEF3 or 0.05 µM ARHGEF12.

Total fluorescence intensities were measured with a Varian Cary Eclipse Fluorescence Spectrophotometer (λ_{ex} = 360 nm, λ_{em} = 440 nm).

Acknowledgements: The authors are indebted to Dr. Daniel Fletcher (College of Life Sciences, University of Dundee), for performing the RMN experiments. PP was supported in part by Tenovus Scotland.

The authors declare no conflict of interest.

APP, CGP, JABC, LV, GF, and JAB participated in writing the publication**.**
GF, JAB, APP, and LV designed the project.
APP, CGP, and LV performed the purification and crystallization**.**
APP and CGP performed the biochemical experiments.
JABC designed and performed the molecular modeling experiments**.**

References

1. Burridge, K., and Wennerberg, K. (2004) Rho and Rac take center stage. *Cell* **116**, 167–179
2. Vega, F. M., and Ridley, A. J. (2016) The RhoB small GTPase in physiology and disease. *Small GTPases.*, 1–10
3. Zandvakili, I., Lin, Y., Morris, J. C., and Zheng, Y. (2016) Rho GTPases: Anti- or pro-neoplastic targets? *Oncogene*
4. Loirand, G., Scalbert, E., Bril, A., and Pacaud, P. (2008) Rho exchange factors in the cardiovascular system. *Curr. Opin. Pharmacol.* **8**, 174–180
5. Loirand, G., and Pacaud, P. (2010) The role of Rho protein signaling in hypertension. *Nat. Rev. Cardiol.* **7**, 637–647
6. Peng, F., Wu, D., Gao, B., Ingram, A. J., Zhang, B., Chorneyko, K., McKenzie, R., and Krepinsky, J. C. (2008) RhoA/Rho-kinase contribute to the pathogenesis of diabetic renal disease. *Diabetes* **57**, 1683–1692
7. Tao, W., Wu, J., Xie, B. X., Zhao, Y. Y., Shen, N., Jiang, S., Wang, X. X., Xu, N., Jiang, C., Chen, S., Gao, X., Xue, B., and Li, C. J. (2015) Lipid-induced Muscle Insulin Resistance Is Mediated by GGPPS via Modulation of the RhoA/Rho Kinase Signaling Pathway. *J. Biol. Chem* **290**, 20086–20097
8. Biro, M., Munoz, M. A., and Weninger, W. (2014) Targeting Rho-GTPases in immune cell migration and inflammation. *Br. J. Pharmacol.* **171**, 5491–5506
9. Koth, A. P., Oliveira, B. R., Parfitt, G. M., Buonocore, J. Q., and Barros, D. M. (2014) Participation of group I p21-activated kinases in neuroplasticity. *J. Physiol Paris* **108**, 270–277
10. Loge, C., Wallez, V., Scalbert, E., Cario-Tourmaniantz, C., Loirand, G., Pacaud, P., and Lesieur, D. (2002) Rho-kinase inhibitors: Pharmacomodulations on the lead compound Y-32885. *J. Enzyme Inhib. Med Chem* **17**, 381–390
11. Smithers, C. C., and Overduin, M. (2016) Structural Mechanisms and Drug Discovery Prospects of Rho GTPases. *Cells* **5**
12. Sanz-Moreno, V., and Marshall, C. J. (2010) The plasticity of cytoskeletal dynamics underlying neoplastic cell migration. *Curr. Opin. Cell Biol.* **22**, 690–696
13. Ridley, A. J. (2006) Rho GTPases and actin dynamics in membrane protrusions and vesicle trafficking. *Trends Cell Biol.* **16**, 522–529
14. Cramer, L. P. (1999) Organization and polarity of actin filament networks in cells: Implications for the mechanism of myosin-based cell motility. *Biochem. Soc. Symp.* **65**, 173–205
15. Jaffe, A. B., and Hall, A. (2005) Rho GTPases: Biochemistry and biology. *Annu. Rev. Cell Dev. Biol.* **21**, 247–269
16. Rossman, K. L., Der, C. J., and Sondek, J. (2005) GEF means go: Turning on RHO GTPases with guanine nucleotide-exchange factors. *Nat. Rev. Mol. Cell Biol.* **6**, 167–180
17. Alberts, A. S., and Treisman, R. (1998) Activation of RhoA and SAPK/JNK signalling pathways by the RhoA-specific exchange factor mNET1. *EMBO J.* **17**, 4075–4085
18. Srougi, M. C., and Burridge, K. (2011) The nuclear guanine nucleotide exchange factors Ect2 and Net1 regulate RhoB-mediated cell death after DNA damage. *PLoS. One.* **6**, e17108
19. Murray, D., Horgan, G., Macmathuna, P., and Doran, P. (2008) NET1-mediated RhoA activation facilitates lysophosphatidic acid-induced cell migration and invasion in gastric cancer. *Br. J. Cancer* **99**, 1322–1329
20. Qin, H., Carr, H. S., Wu, X., Muallem, D., Tran, N. H., and Frost, J. A. (2005) Characterization of the biochemical and transforming properties of the neuroepithelial transforming protein 1. *J. Biol. Chem* **280**, 7603–7613

21. Leyden, J., Murray, D., Moss, A., Arumuguma, M., Doyle, E., McEntee, G., O'Keane, C., Doran, P., and Macmathuna, P. (2006) Net1 and Myeov: Computationally identified mediators of gastric cancer. *Br. J. Cancer* **94**, 1204–1212
22. Ye, K., Chang, S., Li, J., Li, X., Zhou, Y., and Wang, Z. (2014) A functional and protein-protein interaction analysis of neuroepithelial cell transforming gene 1 in hepatocellular carcinoma. *Tumour. Biol.* **35**, 11219–11227
23. Fang, L., Zhu, J., Ma, Y., Hong, C., Xiao, S., and Jin, L. (2015) Neuroepithelial transforming gene 1 functions as a potential prognostic marker for patients with non-small cell lung cancer. *Mol. Med Rep.* **12**, 7439–7446
24. Diviani, D., Raimondi, F., Del Vescovo, C. D., Dreyer, E., Reggi, E., Osman, H., Ruggieri, L., Gonano, C., Cavin, S., Box, C. L., Lenoir, M., Overduin, M., Bellucci, L., Seeber, M., and Fanelli, F. (2016) Small-Molecule Protein-Protein Interaction Inhibitor of Oncogenic Rho Signaling. *Cell Chem Biol.* **23**, 1135–1146
25. Derewenda, U., Oleksy, A., Stevenson, A. S., Korczynska, J., Dauter, Z., Somlyo, A. P., Otlewski, J., Somlyo, A. V., and Derewenda, Z. S. (2004) The crystal structure of RhoA in complex with the DH/PH fragment of PDZRhoGEF, an activator of the Ca(2+) sensitization pathway in smooth muscle. *Structure.* **12**, 1955–1965
26. Kristelly, R., Gao, G., and Tesmer, J. J. (2004) Structural determinants of RhoA binding and nucleotide exchange in leukemia-associated Rho guanine-nucleotide exchange factor. *J. Biol. Chem* **279**, 47352–47362
27. Cierpicki, T., Bielnicki, J., Zheng, M., Gruszczyk, J., Kasterka, M., Petoukhov, M., Zhang, A., Fernandez, E. J., Svergun, D. I., Derewenda, U., Bushweller, J. H., and Derewenda, Z. S. (2009) The solution structure and dynamics of the DH-PH module of PDZRhoGEF in isolation and in complex with nucleotide-free RhoA. *Protein Sci.* **18**, 2067–2079
28. Lenoir, M., Sugawara, M., Kaur, J., Ball, L. J., and Overduin, M. (2014) Structural insights into the activation of the RhoA GTPase by the lymphoid blast crisis (Lbc) oncoprotein. *J. Biol. Chem* **289**, 23992–24004
29. Abdul Azeez, K. R., Knapp, S., Fernandes, J. M. P., Klussmann, E., and Elkins, J. M. (2014) The crystal structure of the RhoA-AKAP-Lbc DH-PH domain complex. *The Biochemical journal* **464**, 231–239
30. Schaefer, A., Reinhard, N. R., and Hordijk, P. L. (2014) Toward understanding RhoGTPase specificity: Structure, function and local activation. *Small GTPases.* **5**, 6
31. Blundell, T. L., Sibanda, B. L., Montalvao, R. W., Brewerton, S., Chelliah, V., Worth, C. L., Harmer, N. J., Davies, O., and Burke, D. (2006) Structural biology and bioinformatics in drug design: Opportunities and challenges for target identification and lead discovery. *Philos. Trans. R. Soc. Lond B Biol. Sci.* **361**, 413–423
32. Kotschy, A., Szlavik, Z., Murray, J., Davidson, J., Maragno, A. L., Le Toumelin-Braizat, G., Chanrion, M., Kelly, G. L., Gong, J. N., Moujalled, D. M., Bruno, A., Csekei, M., Paczal, A., Szabo, Z. B., Sipos, S., Radics, G., Proszenyak, A., Balint, B., Ondi, L., Blasko, G., Robertson, A., Surgenor, A., Dokurno, P., Chen, I., Matassova, N., Smith, J., Pedder, C., Graham, C., Studeny, A., Lysiak-Auvity, G., Girard, A. M., Grave, F., Segal, D., Riffkin, C. D., Pomilio, G., Galbraith, L. C., Aubrey, B. J., Brennan, M. S., Herold, M. J., Chang, C., Guasconi, G., Cauquil, N., Melchiore, F., Guigal-Stephan, N., Lockhart, B., Colland, F., Hickman, J. A., Roberts, A. W., Huang, D. C., Wei, A. H., Strasser, A., Lessene, G., and Geneste, O. (2016) The MCL1 inhibitor S63845 is tolerable and effective in diverse cancer models. *Nature* **538**, 477–482
33. Ma, B., and Nussinov, R. (2014) Druggable orthosteric and allosteric hot spots to target protein-protein interactions. *Curr. Pharm. Des* **20**, 1293–1301
34. Renaud, J. P., Chung, C. W., Danielson, U. H., Egner, U., Hennig, M., Hubbard, R. E., and Nar, H. (2016) Biophysics in drug discovery: Impact, challenges and opportunities. *Nat. Rev. Drug Discov.* **15**, 679–698
35. Dougherty, P. G., Qian, Z., and Pei, D. (2017) Macrocycles as protein-protein interaction inhibitors. *Biochem. J* **474**, 1109–1125

36. Studier, F. W. (2005) Protein production by auto-induction in high density shaking cultures. *Protein Expr. Purif.* **41**, 207–234
37. Page, R., Peti, W., Wilson, I. A., Stevens, R. C., and Wüthrich, K. (2005) NMR screening and crystal quality of bacterially expressed prokaryotic and eukaryotic proteins in a structural genomics pipeline. *Proceedings of the National Academy of Sciences of the United States of America* **102**, 1901–1905
38. Kabsch, W. (2010) XDS. *Acta Crystallogr. D. Biol. Crystallogr.* **66**, 125–132
39. Winn, M. D., Ballard, C. C., Cowtan, K. D., Dodson, E. J., Emsley, P., Evans, P. R., Keegan, R. M., Krissinel, E. B., Leslie, A. G., McCoy, A., McNicholas, S. J., Murshudov, G. N., Pannu, N. S., Potterton, E. A., Powell, H. R., Read, R. J., Vagin, A., and Wilson, K. S. (2011) Overview of the CCP4 suite and current developments. *Acta Crystallogr. D. Biol. Crystallogr.* **67**, 235–242
40. Zwart, P. H., Afonine, P. V., Grosse-Kunstleve, R. W., Hung, L. W., Ioerger, T. R., McCoy, A. J., McKee, E., Moriarty, N. W., Read, R. J., Sacchettini, J. C., Sauter, N. K., Storoni, L. C., Terwilliger, T. C., and Adams, P. D. (2008) Automated structure solution with the PHENIX suite. *Methods Mol. Biol.* **426**, 419–435
41. Adams, P. D., Afonine, P. V., Bunkoczi, G., Chen, V. B., Davis, I. W., Echols, N., Headd, J. J., Hung, L. W., Kapral, G. J., Grosse-Kunstleve, R. W., McCoy, A. J., Moriarty, N. W., Oeffner, R., Read, R. J., Richardson, D. C., Richardson, J. S., Terwilliger, T. C., and Zwart, P. H. (2010) PHENIX: A comprehensive Python-based system for macromolecular structure solution. *Acta Crystallogr. D. Biol. Crystallogr.* **66**, 213–221
42. Emsley, P., and Cowtan, K. (2004) Coot: Model-building tools for molecular graphics. *Acta Crystallogr. D. Biol. Crystallogr.* **60**, 2126–2132
43. Biasini, M., Bienert, S., Waterhouse, A., Arnold, K., Studer, G., Schmidt, T., Kiefer, F., Gallo, C. T., Bertoni, M., Bordoli, L., and Schwede, T. (2014) SWISS-MODEL: Modelling protein tertiary and quaternary structure using evolutionary information. *Nucleic Acids Res* **42**, W252-W258
44. Anandakrishnan, R., Aguilar, B., and Onufriev, A. V. (2012) H++ 3.0: Automating pK prediction and the preparation of biomolecular structures for atomistic molecular modeling and simulations. *Nucleic Acids Res* **40**, W537-W541
45. Jorgensen, W. L., Chandrasekhar, J., Madura, J. D., Impey, R. W., and Klei, M. L. (1983) Comparison of Simple Potential Functions for Simulating Liquid Water. *J. Chem. Phys.* **79**, 926–935
46. Aaqvist, J. (1990) *Ion-water interaction potentials derived from free energy perturbation simulations. J.Phys.Chem.* **94**, 8021–8024
47. Case, D. A., Babin, V., Berryman, J. T., Betz, R. M., Cerutti, D. S., Cheatham, T. E., Darden, T. A., Duke, R. E., Gohlke, H., Goetz, A. W., Gusarov, S., Homeyer, N., Janowski, P., Kaus, J., Kovalenko, A., Lee, T. S., LeGrand, S., Luchko, T., Luo, R., Merz, K. M., Paesani, F., Roe, D. R., Roitberg, A., Sagui, C., Salomon-Ferrer, R., Seabra, G., Simmerling, C. L., Swails, J., Walker, R. C., Wang, J., Wolf, R. M., Wu, X., and Kollman, P. A. (2014) AmberTools15. *University of California, San Francisco, USA*
48. Maier, J. A., Martinez, C., Kasavajhala, K., Wickstrom, L., Hauser, K. E., and Simmerling, C. (2015) ff14SB: Improving the Accuracy of Protein Side Chain and Backbone Parameters from ff99SB. *J Chem. Theory. Comput.* **11**, 3696–3713
49. Darden, T., York, D., and Pedersen, L. (1993) *Particle mesh Ewald: An N·log(N) method for Ewald sums in large systems. J.Chem.Phys.* **98**, 10089–10092
50. Andersen, H. C. (1983) Rattle: A "velocity" version of the shake algorithm for molecular dynamics calculations. *J. Comp. Physics* **52**, 24–34
51. Berendsen, H. J. C., Postma, J. P. M., van Gunsteren, W. F., DiNola, A., and Haak, J. R. (1984) *Molecular dynamics with coupling to an external bath. J.Chem.Phys.* **81**, 3684–3690
52. Delano, W. L. (2002) *DeLano Scientific, San Carlos, California*
53. Humphrey, W., Dalke, A., and Schulten, K. (1996) VMD: Visual molecular dynamics. *J Mol. Graph.* **14**, 33–38

54. Miller, B. R., McGee, T. D., Swails, J. M., Homeyer, N., Gohlke, H., and Roitberg, A. E. (2012) MMPBSA.py: An Efficient Program for End-State Free Energy Calculations. *J Chem. Theory. Comput.* **8**, 3314–3321

Table 1: Analysis of the interactions between RhoA and the DH domains of Net1, RhoGEF11 and RhoGEF12.

The distance corresponds to the distance measured during the 100-ns run in the molecular dynamics (MD) simulations of the interaction between Net1 and RhoA. Residues in italic are not homologous in the superposed structures of Net1, RhoGEF11, and RhoGEF12.

RhoA	Net1 (4XH9)	RhoGEF11 (1XCG)	RhoGEF12 (1X86)	Distance (Å)	Distance measured in MD (Å)
Hydrogen bonds					
R5	Q291	*R868/D873*	*R923*	2.7	4.5 (± 1.0)
T37	E181	E741	E794	2.8	2.8 (± 0.2)
V38	E181	E741	E794	3.1	3.3 (± 0.4)
N41	S306	*Q880*	*Q935*	2.9	4.5 (± 1.3)
D67	N354	N921	N975	3.6	3.6 (± 0.4)
R68	N354	N921	N975	2.9	3.0 (± 0.2)
L69	N354	N921	N975	3.1	3.2 (± 0.3)
E40	S313	*S748*	-	2.7	5.9 (± 0.9)
Q63	R312	-	-	3.1	3.0 (± 0.3)
R68	K357	-	*E982/N983*	2.8	3.0 (± 0.5)
L69	R312	-	-	2.9	3.0 (± 0.3)
L72	W305	-	-	3.6	4.2 (± 0.5)
S73	R312	-	-	2.6	3.0 (± 0.3)
Salt bridges					
E40	K317	R751/R867	R922	3.6	2.9 (± 0.3)
D45	K301	R868	R923	3.9	5.2 (± 1.9)
D76	K274	R872	K899	2.9	3.4 (± 1.0)

Table 2: Analysis of the interactions between RhoA and the PH domains of Net1

Putative Hbond involved in the PH/RhoA interface	Distance measured in 4XH9	Distance measured in MD	Isotropic refinement B factors* (Å^2)		
			Residue / water molecule		Chain
WATER1-H488(Nε2)	3.0	3.0 (± 0.2)	H488	18	
WATER1-E392(O)	2.8	2.8 (± 0.2)	E392	21	**Net1-PH** Average 30 Min 16 Max 64
WATER1-E392(N)	3.3	3.4 (± 0.3)			
WATER1-W492(Nε1)	2.8	3.0 (± 0.2)	W492	17	
WATER2-H390(N)	3.0	3.1 (± 0.3)	H390	18	
H105(Nε2)-H390(O)	2.9	3.2 (± 0.4)	H105	15	**RhoA** Average 28 Min 13 Max 64
WATER1-H105(Nδ1)	3.4	3.7 (± 0.3)	WATER1	16	**Waters** Average 37 Min 14 Max 57
WATER2-H105(Nε2)	2.9	3.3 (± 0.4)	WATER2	22	

*****values represent the AB heterodimer of the asymmetric unit; MD: molecular dynamics

Table 3 Crystallographic data collection and processing

Data collection and processing were conducted at *the European Synchrotron Radiation Facility ESRF (Grenoble, France) on the ID23-1 beamline.*

Parameter	**Value**
Wavelength (Å)	0.97
Temperature (K)	100
Detector: Pilatus 6M	
Crystal-detector distance (mm)	250
Rotation range per image (°)	1
Total rotation range (°)	200
Exposure time per image (s)	0.5
Space group	$P12_11$
a; *b*; *c* (Å)	54.1; 101.4; 116.2
α; β; γ (°)	90.0; 94.3; 90.0
Resolution range (Å)	34.0-2.0 (2.1-2.0)
No. of unique reflections	83900
Completeness (%)	96 (90.4)
Redundancy	3.4 (3.4)
$[I/\sigma(I)]$	13.9 (3.9)
Overall *B* factor from Wilson plot ($Å^2$)	26.3

Values in parentheses represent the outer shell.

†estimated by multiplying the conventional R_{merge} value by the factor $[N/(N-1)]^{1/2}$

Table 4: Crystallographic structure solution and refinement

Parameter	**Value**
Resolution range (Å)	35.0-2.0
Completeness (%)	99.4
σ cutoff	2.0
No. of reflections, working set	83896
No. of reflections, test set	4194
Final R_{cryst}	0.18
Final R_{free}	0.21
Cruickshank DPI	
No. of non-H atoms	9206
Protein	8269
Water	921
Total	
RMSDs	
Bonds (Å)	0.012
Angles (°)	1.39
Average *B* factors (Å^2)	35
Protein	29
Water	78
Ramachandran plot	
Most favored (%)	97.2
Allowed (%)	2.4

RMSDs: root mean square deviations

Figure Legends

Figure 1: Purification of the Net1^{DHPH}/RhoA complex

(A) Superdex S200 26-60 gel-filtration profile of the Net1^{DHPH}/RhoA complex. (B) Coomassie-stained SDS-PAGE gel shows the Net1^{DHPH}/RhoA complex isolated with Superdex S200 chromatography. MW markers.10, 15, 25, 35, 45, 67, 90 kDa; Lane 1: the higher band is the Net1/RhoA complex; Lane 2: lower band shows excess unbound RhoA.

Figure 2: Overall crystal structure of RhoA/Net1^{DHPH} complex

RhoA is shown in orange; switch 1 is in purple and switch 2 is in green (30). The Net1 DH domain is in cyan and the Net 1 PH domain is in yellow.

Figure 3: Superposition of the RhoA structure from the Net1^{DHPH}/RhoA complex with a bound GDP structure suggests the likely binding site for GDP.

The RhoA (orange, with cyan side-chains) from the Net1^{DHPH}/RhoA structure (PBD code **4XH9**) is superposed onto the GDP (purple, with a red pyrophosphate) from the RhoA/GDP structure (PDB code **4D0N**).

Figure 4: Comparison of Net1^{DHPH} (PDB code 4XH9) and Net1^{DH} (PDB code 3EO2) structures.

(A) Calculated RMSDs for Net1^{DHPH} and Net1^{DH}. The main chain deviations calculated with PROGRAM are indicated for each residue (circles). (B) Alignment of Net1^{DHPH} (blue/yellow) and Net1^{DH} (magenta) structures. RhoA is shown in orange. (C) Close-up view of the alignment of Net1^{DHPH} (cyan, with blue side-chains) and Net1^{DH} (magenta, with magenta side-chains) structures shows that D309 could not be involved in RhoA binding to Net1, due to the clash between S306/D309 from Net1 and W58 from RhoA (green).

Figure 5: The DH/RhoA interface

(A) DH residues (blue) involved in the interface. B) RhoA residues (magenta) involved in the interface. RhoA is shown in orange, DH in cyan.

Figure 6: **Conformational distributions of the DH/PH domains of Net1.** Molecular dynamics results show the root mean square deviation (RMSD) of the α6 helix (residues 357-368) on the X-axis (Å), and the DH/PH angle (i.e., the angle between the Cα carbons of residues Q337, L355, and I496) on the Y-axis (degrees). Each plot shows representative structures of Net1; the α6 and αC helices are shown in cyan and yellow cylinders,

respectively. The color scale indicates the number of occurrences per bin normalized to the maximum number in a bin (A) Net1 in complex with RhoA; (B) Net1 in the absence of RhoA

Figure 7: Biochemical characterization of GTP/GDP exchange activities for the Net1/RhoA complex.

. RhoA exchange activity was measured in the presence of the DHPH segment of Net1 (1 µM, dark circles). The GTP/GDP exchange activity of Net1 DH (10 µM) is shown as control experiment (half-tone symbols). The experiments were run at least 3 times, independently. A representative curve is presented here.

Figure 8: **The PH/RhoA interface**

(A) Structural alignment of the PH domains in Net1$^{\mathbf{DHPH}}$ (yellow/blue), RhoGEF11 (brown), and RhoGEF12 (green). Net1 corresponding residues based on the sequences alignement are shown in sticks.

(B) The Net1 PH/RhoA interface; interactions between side-chains are shown for the Net1 DH (cyan) and PH domains (yellow) and RhoA (orange).

Figure 9: Net1PH/RhoA heterodimer formation analysis

(**A**) NMR data show the protein complex (200 µL at a concentration of 1.8 mg/mL, 104.8 µM) in 20 mM Tris, 200 mM NaCl, 10% glycerol, 1 mM TCEP, pH 7.5, mixed with 20 µL D2O, and placed in a 3-mm NMR tube. (**B**) Superdex S75 10/300 gel-filtration profile of Net1^{PH} (orange), RhoA (green), and Net1^{PH} pre-incubated with RhoA at a ratio of 1:1 (pink) or 2:1 (blue). The eluted fractions (1-7) are indicated with red numbers. The peak observed at 17 mL corresponds to the GDP present in the RhoA buffer. (**C**) TGX Stain-free SDS-PAGE gel of the elution fractions from the Net1^{PH} RhoA gel-filtration run (ratio 2:1). Lane 1: Net1^{PH}, fraction 6; Lane 2: RhoA, fraction 4; Lane 3: Molecular weight markers: 10, 15, 20, 25, 37, 50, 75, 100, 150, 250 kDa; Lanes 4-10. Elution fractions 1-7 from Net1^{PH} RhoA (ratio 2:1; blue trace in panel A)

.

Figure 10: **MM-GBSA per residue decomposition analysis of the Net1 PH domain (*top*) and the RhoA (*bottom*) complex.** The total binding free energy contribution is shown for each amino acid residue, and those with the highest contributions are highlighted. MM-GBSA: molecular mechanics energies combined with the generalized Born and surface area continuum solvation

Figure 11: Biochemical characterization of the inhibitory effect of peptides on the Net1/RhoA GTP/GDP exchange reaction

(A) Schematic representation of the inhibitor peptides. The peptide names (*left*) include number ranges that correspond to the amino acid sequences (*right*). (B) Inhibition of Net1-mediated RhoA GTP/GDP exchange with different inhibitor peptides (all at 0.5 mM). Symbols (from top to bottom): closed circles: no peptide, open circles: peptide 100-105, upward triangles: peptide 100-109, stars: peptide 96-102, large upward triangles: peptide 96-106, downward triangles: peptide 101-106, diamonds: peptide 102-106 and squares: peptide 100-106. (C) Inhibition of Net1-mediated RhoA GTP/GDP exchange with different concentrations of peptide 102-106: Symbols from top to bottom: circles: no peptides (control), stars: 0.03 mM, diamonds: 0.0625 mM, downward triangles: 0.125 mM, upward triangles: 0.35 mM and squares: 0.5 mM. The experiments were run at least 3 times, independently. A representative curve is presented here.

Figure 12: Biochemical characterization of GTP/GDP exchange activities for GEF3/RhoA, and GEF12/RhoA complexes

(A) GEF3-mediated RhoA GTP/GDP exchange reaction is not inhibited by 0.5 mM inhibitor peptide 102-106. RhoA exchange activity was measured in the presence of GEF3 (10 µM, dark triangles) or in the presence of both GEF3 (10 µM) and peptide 102-106 (0.5 mM, open triangles). (B) GEF12-mediated RhoA GTP/GDP exchange reaction is not inhibited by 0.5 mM inhibitor peptide 102-106. RhoA exchange activity was measured in the presence of GEF12 (0.05 µM, dark squares) or in the presence of both GEF12 (0.05 µM) and peptide 102-106 (0.5 mM, open squares). The experiments were run at least 3 times, independently. A representative curve is presented here.

Figure 13: Sequence alignment of Net1, GEF3, and GEF12.

Amino acid sequences of $Net1^{PH}$, GEF3, and GEF12 were aligned with the EMBL-EBI Clustal Omega. Secondary structure attributions for $Net1^{PH}$ (PDB: 4XH9; indicated above the corresponding sequences) were identified with the DSSP program. Residues involved in the $Net1^{PH}$/RhoA formation are enclosed in boxes.

Figure 14: Further biochemical characterization of the peptide 102-106 inhibition of the GTP/GDP exchange activities for mutated Net1/RhoA, and GEF3/RhoA.

(A) The Net1-mediated RhoA GTP/GDP exchange reaction is measured in the presence (open symbols) or not (dark symbols) of 0.5 mM of the peptide 102-106. Mutated Net1 (H488N – diamonds - or H488A -circles) were used in those assay together with RhoA. (B) The

GEF3(N436H) mutant-mediated RhoA GTP/GDP exchange reaction is measured in the presence (open symbols) or not (dark symbols) of 0.5 mM of the peptide 102-106. The experiments were run at least 3 times, independently. A representative curve is presented here.

Figure 1

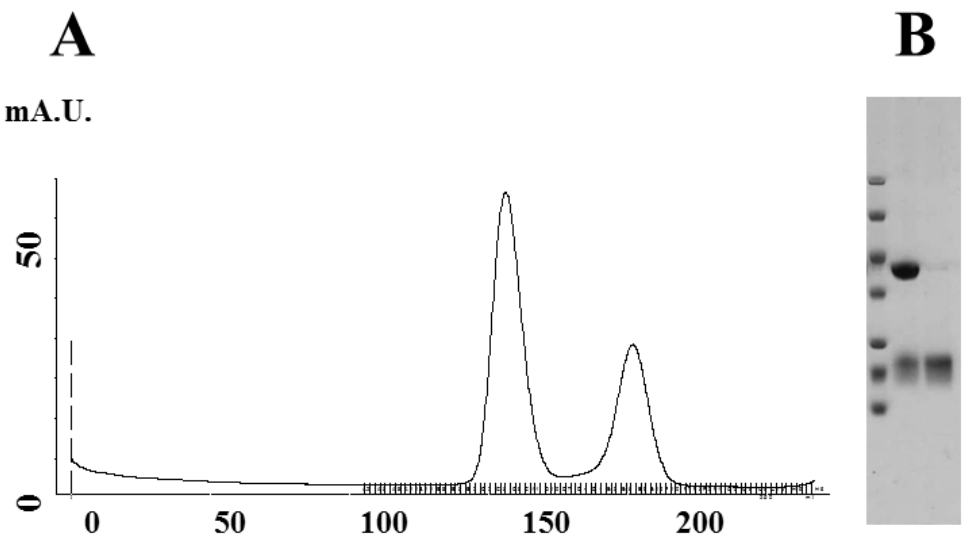

Figure 2.

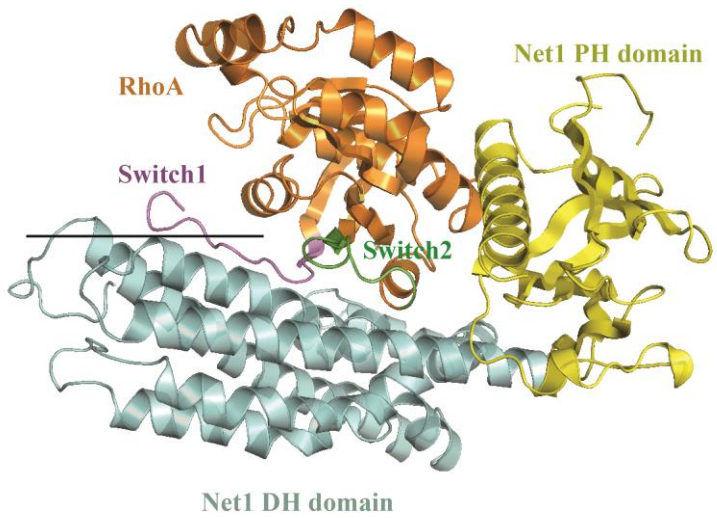

Figure 3.

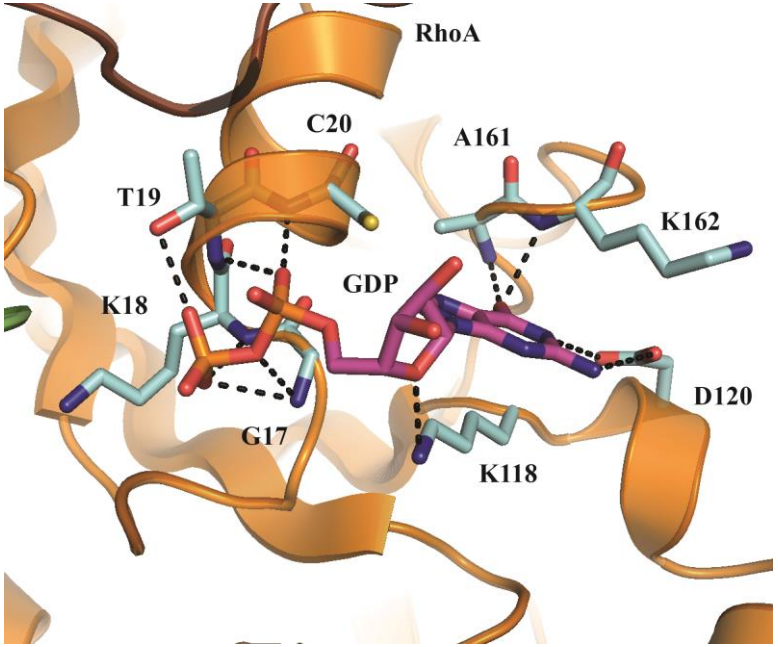

Figure 4.

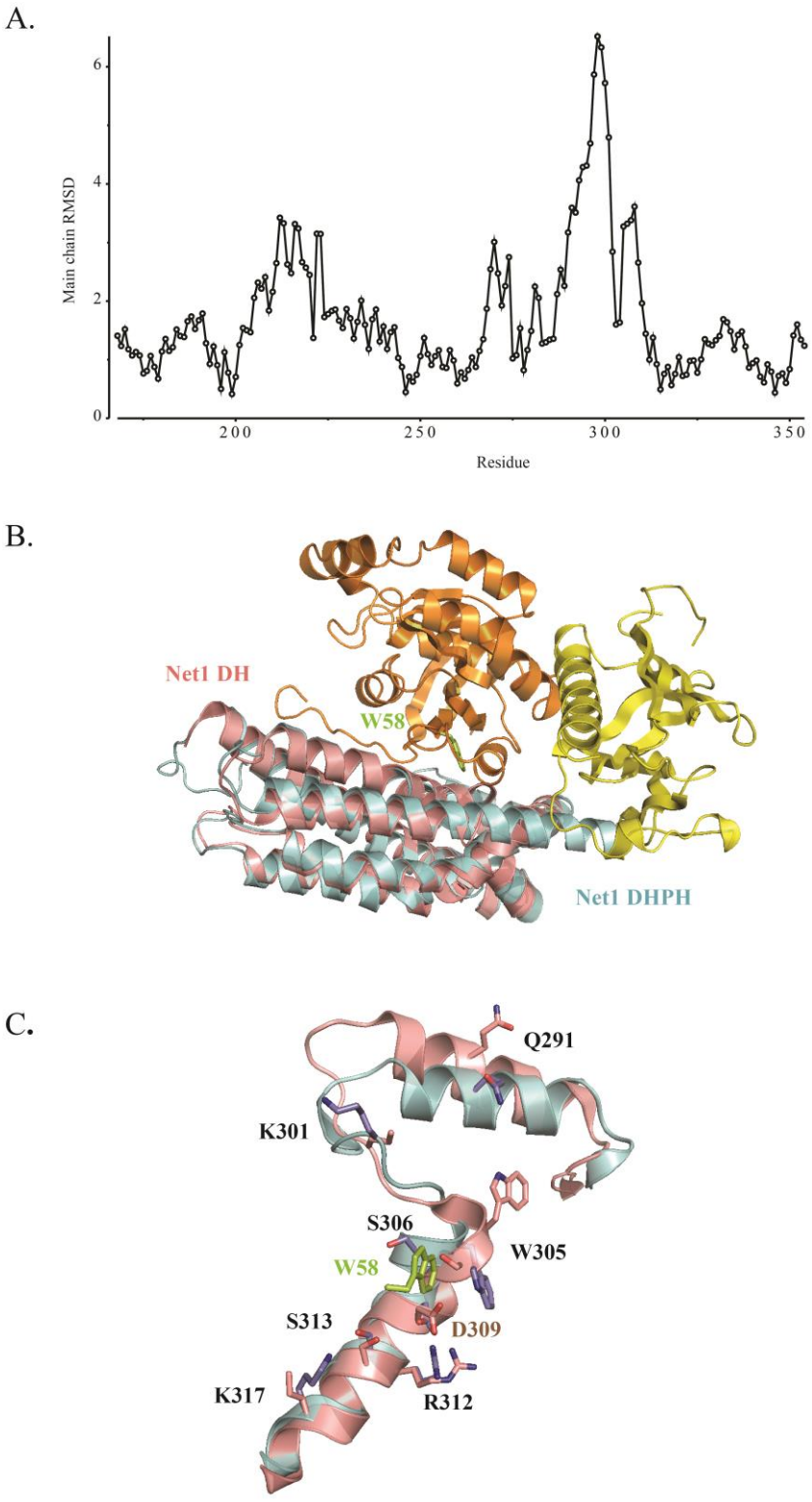

Figure 5.

A.

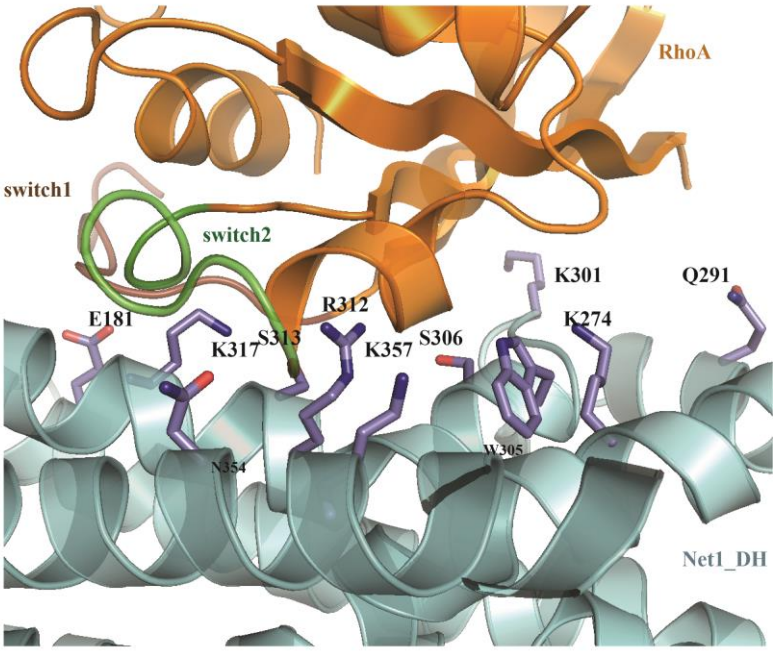

B.

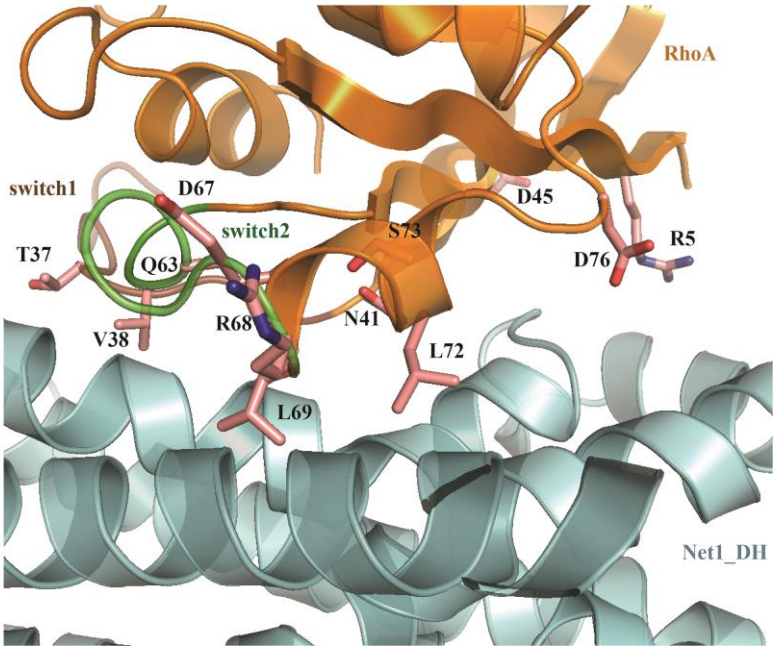

Figure 6.

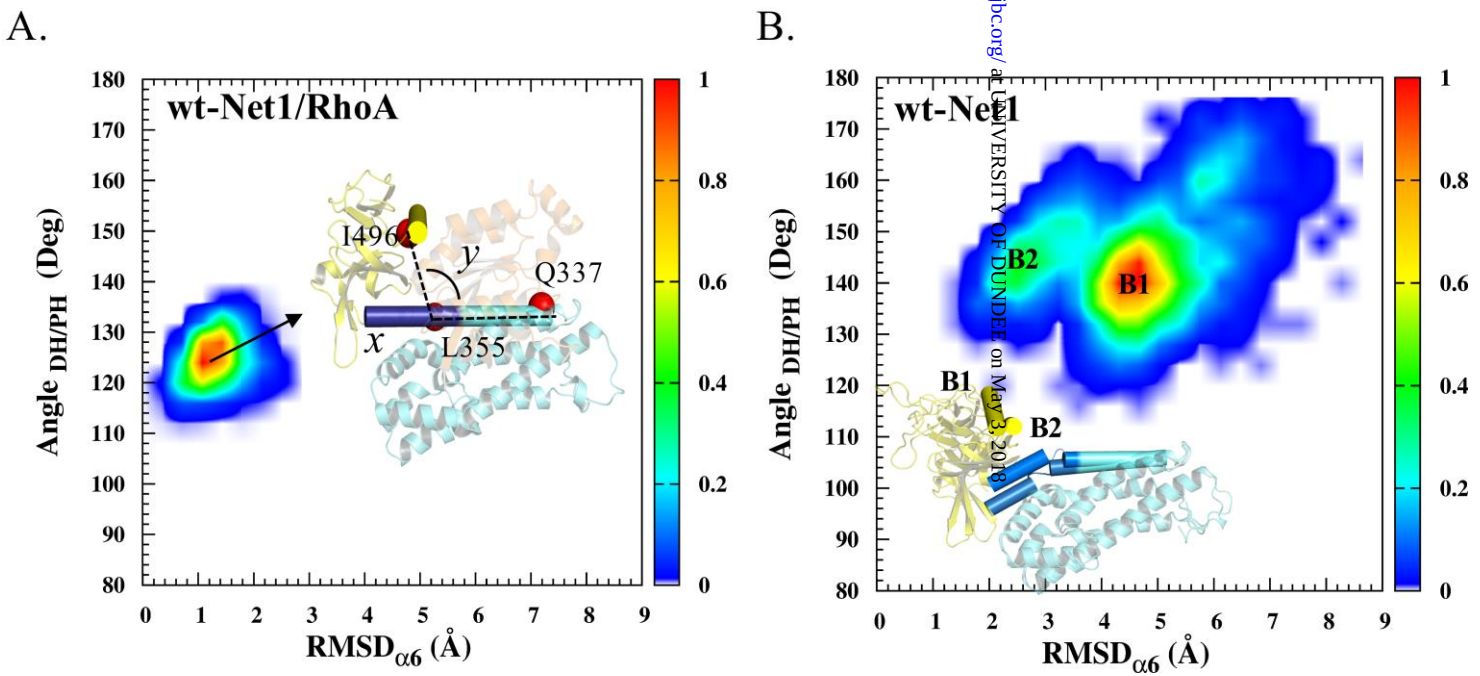

Figure 7.

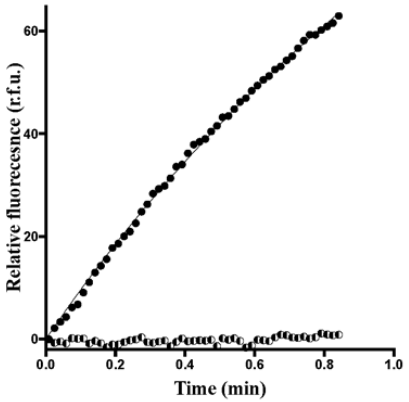

Figure 7

Figure 8.

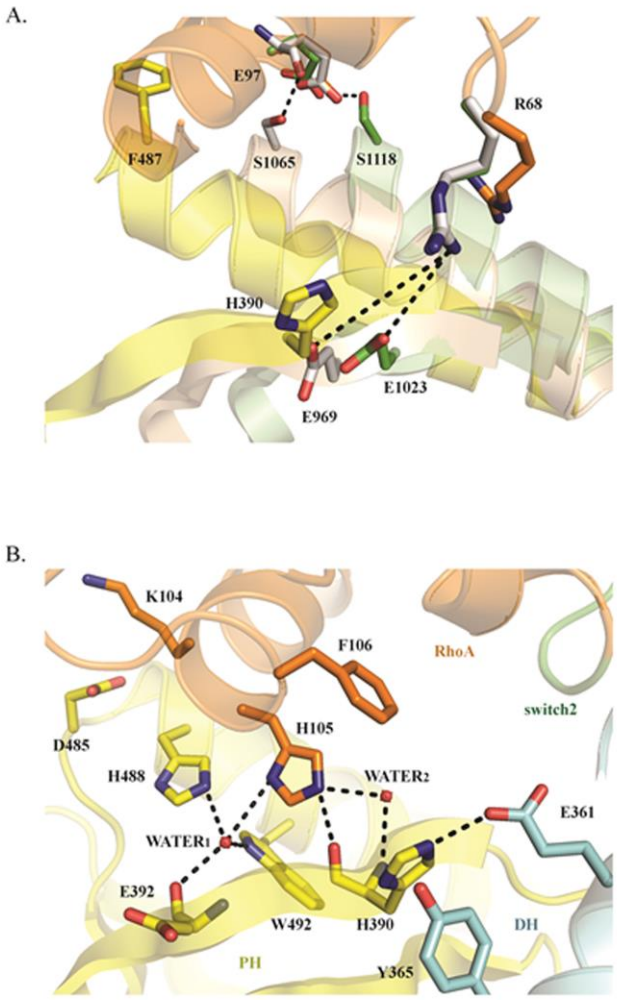

Figure 8

Figure 9.

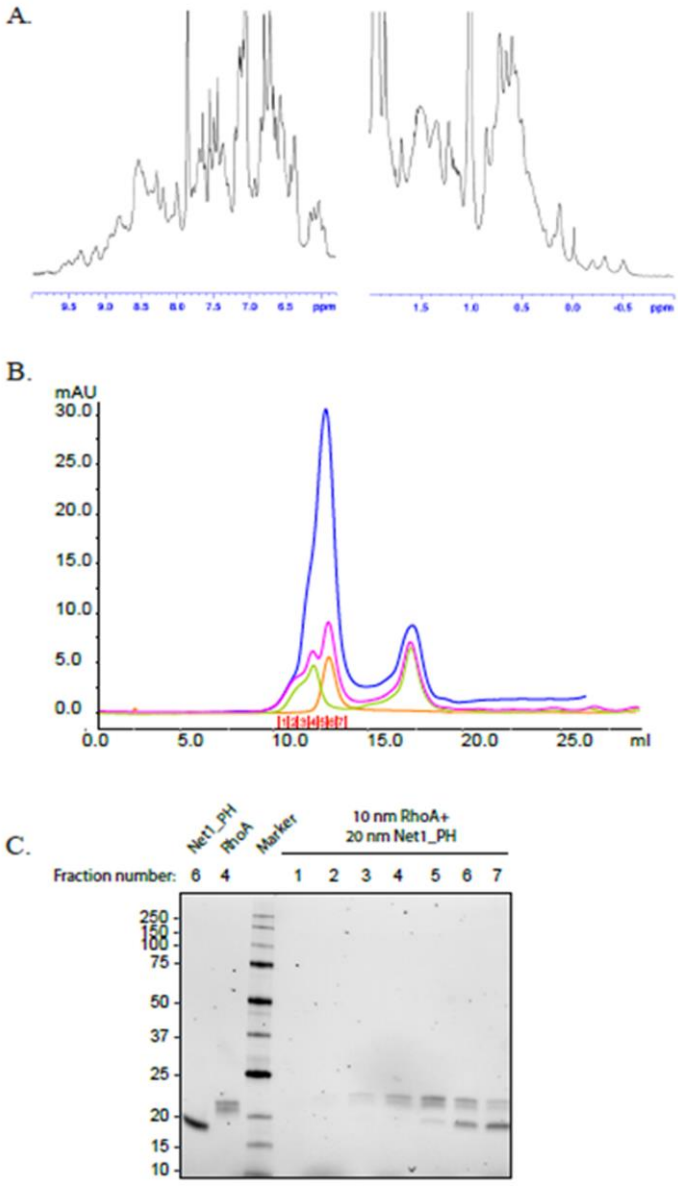

Figure 10.

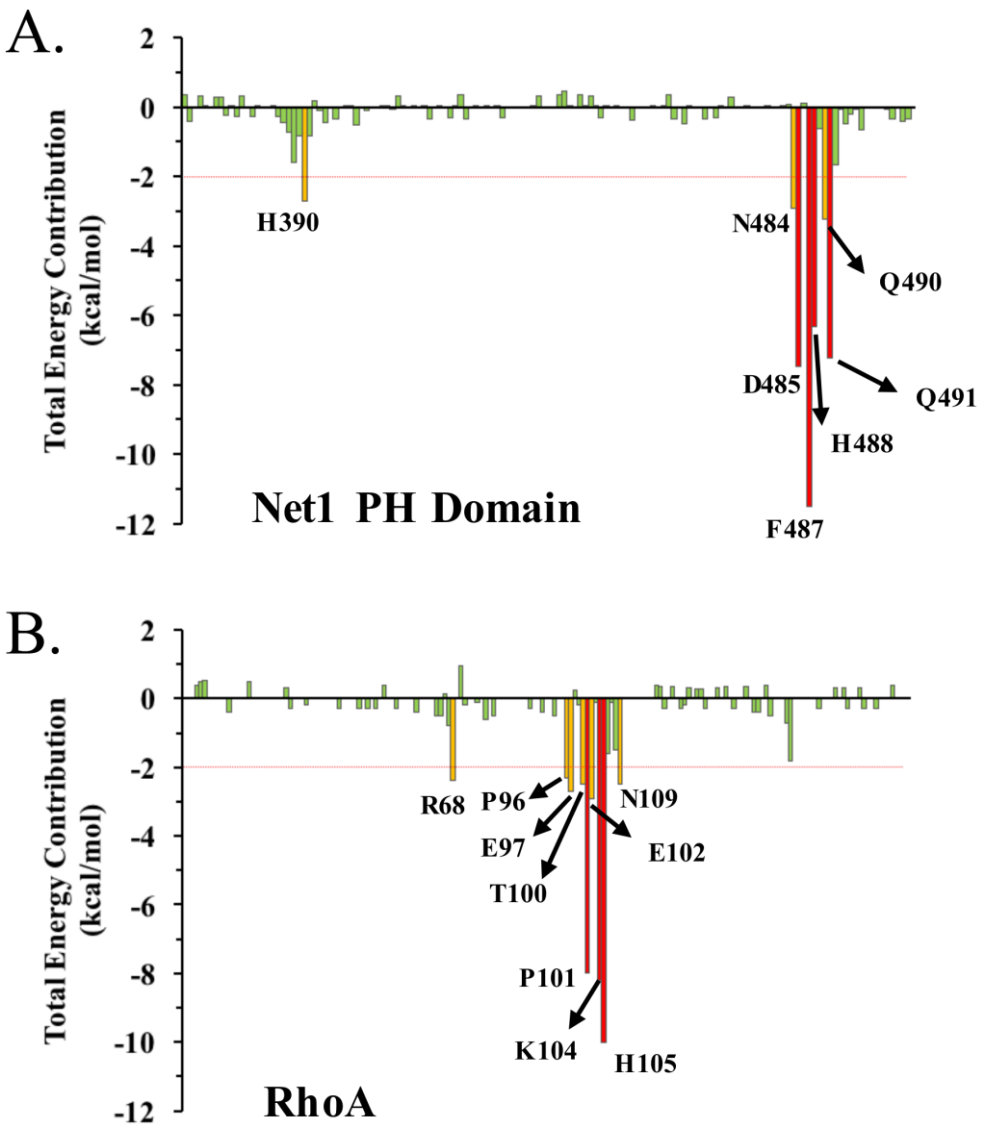

Figure 11.

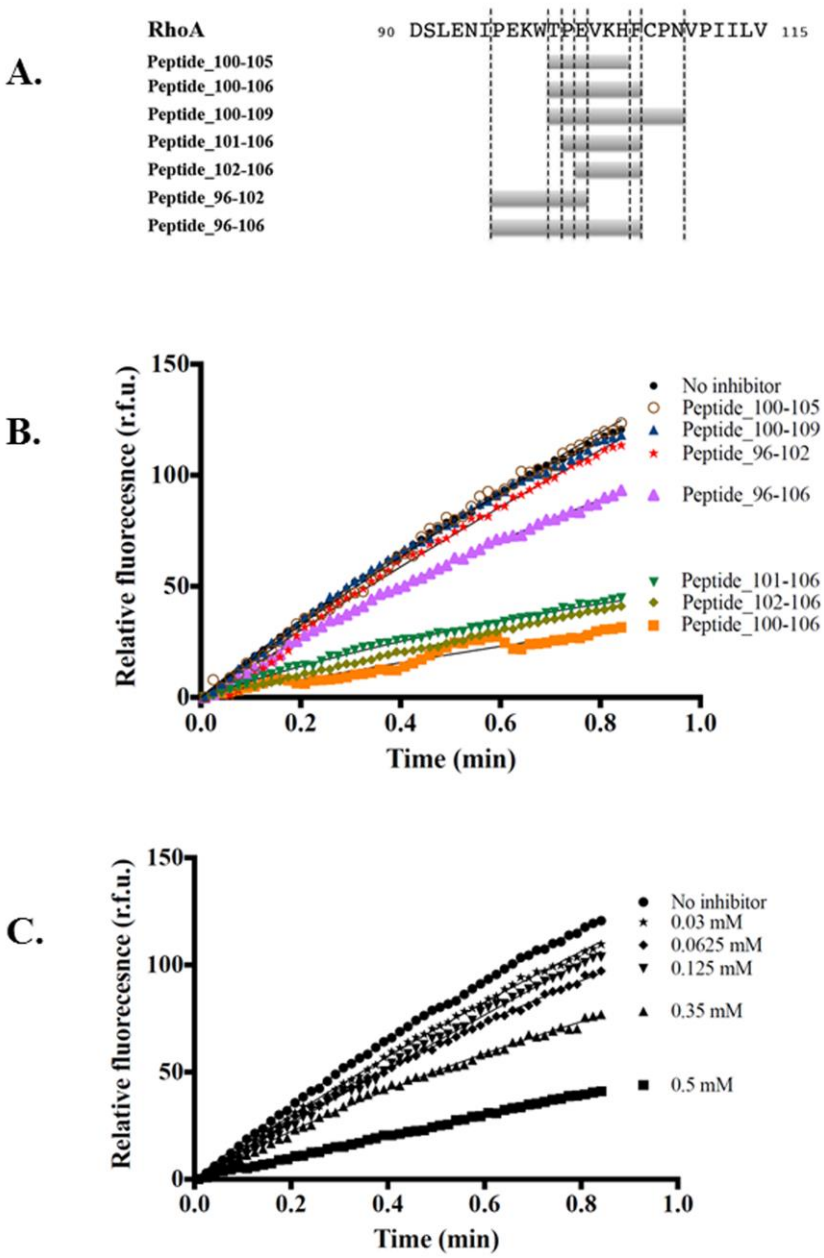

Figure 12.

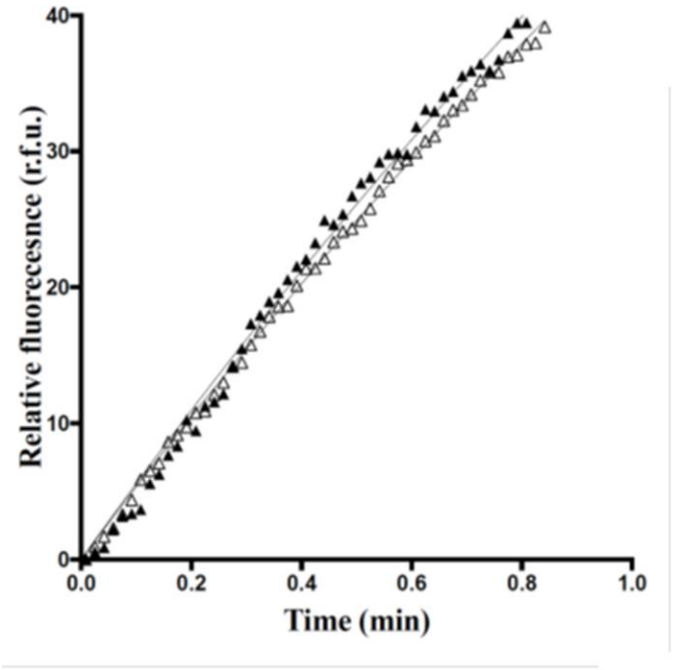

A

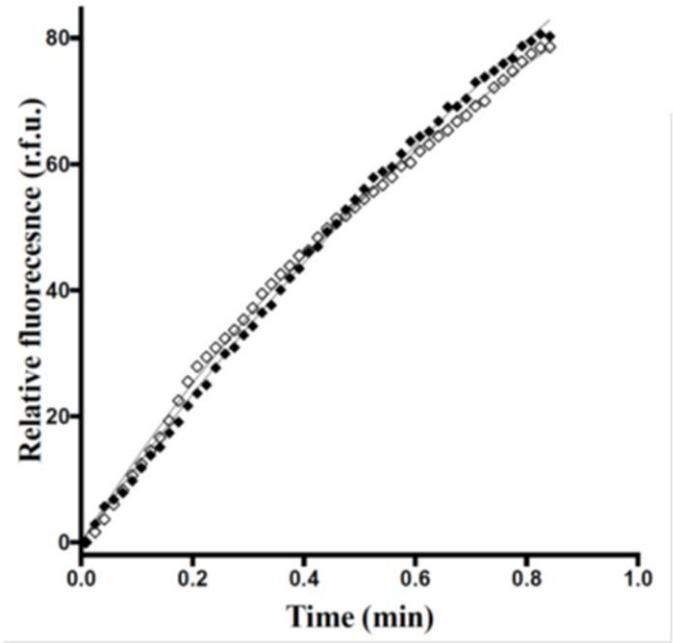

B

Figure 12

Figure 13.

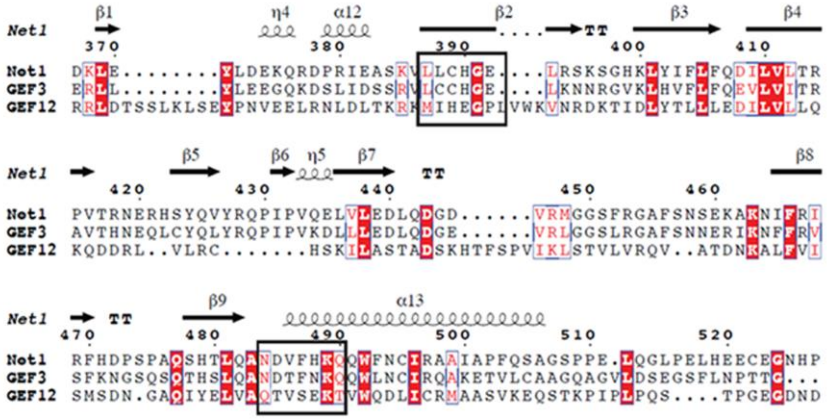

Figure 13

Figure 14.

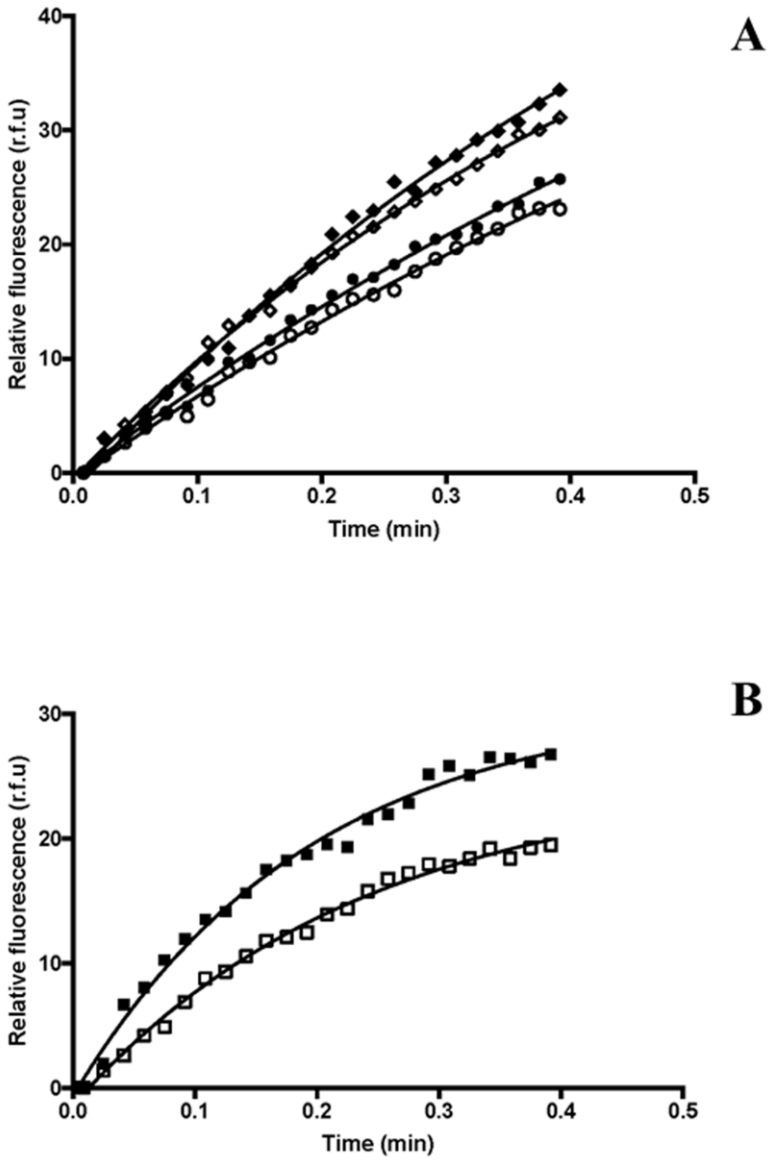

Figure 14

A structural study of the complex between neuroepithelial transforming gene 1 (Net1) and RhoA reveals a potential anti-cancer drug hotspot

Alain-Pierre Petit, Christel Garcia-Petit, Juan A. Bueren-Calabuig, Laurent M. Vuillard, Gilles Ferry and Jean A. Boutin

J. Biol. Chem. published online April 25, 2018
